Title

Functional capacity of XRCC1 protein variants identified in DNA repair-deficient Chinese hamster ovary cell lines and the human population

Journal

Nucleic Acids Research, 38(15)

ISSN

0305-1048

Authors

Berquist, Brian R
Singh, Dharmendra Kumar
Fan, Jinshui
et al.

Publication Date

2010-08-01

DOI

10.1093/nar/gkq193

Published online 12 April 2010 *Nucleic Acids Research, 2010, Vol. 38, No. 15* ***5023–5035***
doi:10.1093/nar/gkq193

Functional capacity of XRCC1 protein variants identified in DNA repair-deficient Chinese hamster ovary cell lines and the human population

Brian R. Berquist[1], Dharmendra Kumar Singh[1], Jinshui Fan[2], Daemyung Kim[3], Elizabeth Gillenwater[4], Avanti Kulkarni[5], Vilhelm A. Bohr[1], Eric J. Ackerman[6], Alan E. Tomkinson[2] and David M. Wilson III[1,*]

[1]Laboratory of Molecular Gerontology, National Institute on Aging, NIH, Baltimore, MD 21224, [2]Department of Radiation Oncology, University of Maryland School of Medicine, Baltimore, MD 21201, USA, [3]Department of Genetic Engineering, Cheongju University, Cheongju 360-764, Republic of Korea, [4]University of Maryland School of Medicine, Baltimore, MD 21201, [5]Department of Radiation Oncology, UCSF School of Medicine, San Francisco, CA 94103 and [6]Department of Nanobiology, Sandia National Laboratories, Albuquerque, NM 87123, USA

Received August 9, 2009; Revised February 26, 2010; Accepted March 8, 2010

ABSTRACT

XRCC1 operates as a scaffold protein in base excision repair, a pathway that copes with base and sugar damage in DNA. Studies using recombinant XRCC1 proteins revealed that: a C389Y substitution, responsible for the repair defects of the EM-C11 CHO cell line, caused protein instability; a V86R mutation abolished the interaction with POLβ, but did not disrupt the interactions with PARP-1, LIG3α and PCNA; and an E98K substitution, identified in EM-C12, reduced protein integrity, marginally destabilized the POLβ interaction, and slightly enhanced DNA binding. Two rare (P161L and Y576S) and two frequent (R194W and R399Q) amino acid population variants had little or no effect on XRCC1 protein stability or the interactions with POLβ, PARP-1, LIG3α, PCNA or DNA. One common population variant (R280H) had no pronounced effect on the interactions with POLβ, PARP-1, LIG3α and PCNA, but did reduce DNA-binding ability. When expressed in HeLa cells, the XRCC1 variants—excluding E98K, which was largely nucleolar, and C389Y, which exhibited reduced expression—exhibited normal nuclear distribution. Most of the protein variants, including the V86R POLβ-interaction mutant, displayed normal relocalization kinetics to/from sites of laser-induced DNA damage: except for E98K and C389Y, and the polymorphic variant R280H, which exhibited a slightly shorter retention time at DNA breaks.

INTRODUCTION

Once thought to be an extraordinarily stable molecule, DNA is now recognized to be susceptible to both spontaneous decay and attack from a number of chemical agents, most notably endogenous reactive oxygen species (1). The most common forms of DNA damage, particularly under normal physiological conditions (i.e. in the absence of environmental challenges), are base modifications, abasic (AP) sites and single-strand breaks (SSBs). If unrepaired, such genetic damage can lead to inaccurate copying of the genome, chromosome instability, and blockage of transcription or replication. Such outcomes can impede the normal function of the cell and give rise to disease. Indeed, defects in DNA damage responses have been associated with cancer predisposition, cognitive decline and premature aging disorders (2–4).

The major repair pathway responsible for handling the most common forms of DNA damage is base excision repair (BER) (5). In brief, this process involves the excision of a base lesion, incision at the resulting AP site, clean-up of the SSB, gap-filling and sealing of the remaining nick. A prominent participant in the repair of DNA SSBs is X-ray cross-complementing 1 (XRCC1), a non-enzymatic factor that operates as a scaffold protein during the repair response (6). XRCC1 has biologically significant interactions with the DNA strand break sensor poly(ADP-ribose) polymerase 1 (PARP-1), the gap-filling DNA polymerase β (POLβ), the DNA 3′-phosphatase (PNKP) and DNA ligase 3α (LIG3α) (7–11). In addition to its repair functions during the G(1) cell cycle phase, XRCC1 operates in unique, yet undefined ways to facilitate S-phase, replication-associated repair events (12–16). Defects in XRCC1 are connected

*To whom correspondence should be addressed. Tel: +1 410 558 8153; Fax: +1 410 558 8157; Email: wilsonda@mail.nih.gov

with increased sensitivity to a number of DNA-damaging agents [e.g. methylmethane sulfonate (MMS) and ionizing radiation (IR)], compromised SSB repair (SSBR), and elevated sister chromatid exchange (6,17).

Deficiencies in human BER have been causally associated with cancer susceptibility or disease development. For instance, mutations in the MutY DNA glycosylase, MYH, or in the nuclear uracil DNA glycosylase, UNG, are genetically linked to colorectal cancer or hyper-IgM syndrome, respectively (18,19). More indirect correlations of defective BER and disease risk have been suggested for POLβ variants, which are detected in a high percentage of tumors and exhibit mutator characteristics (20). In the case of XRCC1, a large number of single nucleotide polymorphisms (SNPs) that affect amino acid composition have been reported in the human population, and epidemiology studies have found an association of some of these with cancer risk (21–23). However, little is known about the molecular repair capacity of the altered XRCC1 proteins, and the epidemiological association studies have often been inconclusive or contradictory. In addition to the human variants, XRCC1 mutations have been identified in Chinese hamster ovary (CHO) cell lines that exhibit increased sensitivity to DNA-damaging agents as well as genomic instability (24).

To define the repair capacity of XRCC1 amino acid variants, we purified a select group of proteins and examined their *in vitro* interaction capacities with a number of associating BER protein partners, as well as with DNA. In addition, following transient transfection into HeLa cells, we determined the localization and response dynamics of fluorescent-tagged versions of the proteins to and from sites of laser-induced DNA damage. We report herein the results of nine human XRCC1 variant proteins: V86R and R109A, predicted by structural analysis to affect POLβ and/or DNA binding (25,26); E98K (≈E102K in CHO) and C389Y (≈C390Y in CHO), identified in the repair-deficient hamster cell lines EM-C12 and EM-C11, respectively (24); and P161L, R194W, R280H, R399Q and Y576S, found within the population, and in some instances, associated with disease susceptibility (21,27). Our data unveil the molecular defects of XRCC1 in the mutant EM-C11 and EM-C12 CHO cell lines, and provide novel insights into the functional consequences of amino acid substitutions found within the population.

MATERIALS AND METHODS

Creation of site-specific XRCC1 amino acid variant constructs

The variants R194W and R399Q were created using an overlapping PCR technique (28). In brief, product 1 (P1), which was designed to harbor the site-specific mutation for R194W, was produced by standard PCR amplification using primers X15′Eco and X1Arg194Trp (Table 1), and a wild-type (WT) XRCC1 cDNA template (14). Unmodified product 2 (P2) was generated via PCR amplification using primers X1prod1 and X13′Xba (Table 1). For R399Q, mutation-containing P1 was produced using X1Arg399Gln and X13′Xba, and unmodified P2 was created with X15′Eco and X1prod2 (Table 1). In either case, P1 was mixed with P2 at a 10:1 ratio, and a third round of PCR was executed using X15′Eco and X13′Xba. This final full-length PCR product was subsequently digested with EcoRI and XbaI, and subcloned into the corresponding restriction sites of pcDNA3 (Invitrogen,

Table 1. Oligonucleotides used for the studies herein

Name	Oligonucleotide sequence (5′–3′)
X15′Eco	CGGAATTCACCATGCCGGAGATCCGCCTCCG
X1Arg194Trp	ATGTCTTGTTGATCCAGCTGAAGAAGAG
X1prod1	GCAGCCAGCCCTACAGCAAGGA
X13′Xba	GCTCTAGATCAGGCTTGCGGCACCACCC
X1Arg399Gln	CACCGCATGCGTCAGCGGCTGCCCTCC
X1prod2	CCTCAAAGCTGGGATCCCATT
5′X1BlgN	GAAGATCTCACCATGCCGGAGATCCGCCTCCG
3′XEcoN	CGGAATTCGGGCTTGCGGCACCACCCCAT
Variant	Primer set and sequence (5′–3′)
E98K	X1E102Kfor: ATG TCC CCT TCC AAG AGC CGC AGT GGC X1E102Krev: GCC ACT GCG GCT CTT GGAAGG GGA CAT
P161L	X1Pro161Leufor: GAG GCA GAG GCC CTG TCC CAG AAG GTG X1Pro161Leurev: CAC CTT CTG GGA CAG GGC CTC TGC CTC
R280H	X1Arg280Hisfor: CCA GCT CCA ACT CAT ACC CCA GCC ACA G X1Arg280Hisrev: CTG TGG CTG GGG TAT GAG TTG GAG CTG G
C389Y	X1C390Yfor: TGG GTG CTG GAC TAT CAC CGC ATG CGT X1C390Yrev: ACG CAT GCG GTG ATA GTC CAG CAC CCA
Y576S	X1Tyr576Serfor: GAG CTC GAG GAC TCT ATG AGT GAC CGG X1Tyr576Serrev: CCG GTC ACT CAT AGA GTC CTC GAG CTC

Top, oligonucleotides employed for the overlapping PCR mutagenesis or for specific DNA fragment amplication. Bottom, primer sets used with the QuikChange mutagenesis kit. The amino acid substitution is listed to the left. The forward (for) and reverse (rev) primer name and its nucleotide sequence are provided in the column to the right. Name and nucleotide sequence are denoted.

Carlsbad, CA). Following sequence verification, mutant-containing inserts were re-amplified and subcloned into pET29a (Novagen/EMD Chemicals, Gibbstown, NJ) as described for WT XRCC1 (14). XRCC1 mutants V86R and R109A, which were designed previously (9), were transferred from pcDNA3 to pET29a in an identical manner. All plasmid sequences were confirmed by Lark Technologies (Houston, TX) prior to use.

Human XRCC1 variants E98K, P161L, R280H, C389Y and Y576S were created using the QuikChange II Site-Directed Mutagenesis Kit (Stratagene, La Jolla, CA). In brief, the forward primer and the reverse primer (125 ng each; Table 1) were mixed with 10 ng XRCC1-pET29a plasmid (14), dNTPs, and PfuUltra HF DNA Polymerase to generate recombinant plasmids harboring the desired nucleotide substitution. Plasmids were then digested by *Dpn*I, which cuts methylated and hemimethylated DNA, to eliminate WT plasmids (see manufacturer protocol for details). The remaining, undigested plasmids were transformed into XL1-blue cells (Stratagene), and individual clones were sequence verified by Lark Technologies.

The WT, yellow fluorescent protein (YFP)-tagged pXRCC1-EYFP expression construct has been described previously (14). To create the protein variant constructs, an XRCC1 cDNA harboring the V86R, E98K, R109A, P161L, R194W, R280H, C389Y, R399Q or Y576S substitution was PCR amplified from the corresponding pET29a recombinant plasmid described above using primers 5′X1BLgN and 3′XEcoN (Table 1). These inserts were subsequently digested with *Bgl*II and EcoRI, and subcloned into the identical restriction sites within pEYFP-N1 (Clontech, Mountain View, CA). All recombinant plasmids were sequence confirmed by Johns Hopkins synthesis and sequencing facility (Baltimore, MD).

Purification of recombinant proteins

pET29a expression plasmids containing an XRCC1 cDNA (WT or variant, see above) were transformed into *Escherichia coli* strain BL21 (λDE3) (Novagen). Each protein harbors an N-terminal S-peptide tag and a C-terminal hexahistidine-tag. Purification of the recombinant proteins was performed essentially as described (14), except protein expression after IPTG induction proceeded overnight at 20°C. Recombinant DNA POLβ, PCNA and PARP-1 were purified as described previously (29–31).

For the purification of DNA LIG3α, cell cultures of *E. coli* strain BL21 (λDE3) harboring pGex plasmids expressing human LIG3α (subcloned into the BamH1 and SalI restriction sites) with a GST tag at the N-terminus (32) were grown at 37°C to a density of 0.9 at OD_{600}. Protein induction was initiated by adding IPTG to a final concentration of 1 mM and continued at 9°C overnight. GST-tagged LIG3α was purified using GST•Bind beads (Novagen) according to the manufacturer's instructions. Briefly, the pellet from a 150 ml cell culture was suspended in 6 ml GST bind/wash buffer (4.3 mM Na_2HPO_4, 1.47 mM KH_2PO_4, 137 mM NaCl, 2.7 mM KCl, pH 7.3). Cells were then lysed by sonication, followed by centrifugation at 36 000× *g* for 20 min at 4°C. The clarified cell extracts were brought to room temperature and loaded onto a column that was packed with 0.5 ml GST•Bind beads and equilibrated with GST bind/wash buffer (see details from manufacturer). After the cell extracts were passed through the column via gravity, the column was washed with 10 ml GST bind/wash buffer. LIG3α protein was eluted with 1.5 ml GST elution buffer (10 mM reduced glutathione in 50 mM Tris, pH 8.0) and stored in aliquots at −80°C until needed.

Protein–protein interaction assay

To determine the interaction affinity of XRCC1 for a specific protein partner, 4 μg of S-peptide-tagged XRCC1 was incubated with S-protein-agarose (Novagen) on ice for 1 h with constant mixing. The matrix was then washed twice with binding buffer (50 mM HEPES–KOH, pH 7.5, 150 mM KCl, 0.02 mM EDTA, 1 mM DTT, 10% glycerol, 0.015% Triton X-100) to remove unbound material (14), and an amount of target protein determined to be within the linear range of binding capacity (typically around 25%) was incubated at 4°C for 1 h with constant mixing in 50 μl of binding buffer (1 or 2 μg POLβ, 1 μg LIG3α, 3 μg PCNA and 2 μg PARP-1). The S-protein-agarose was pelleted by centrifugation, washed four times with 200 μl binding buffer, and resuspended in SDS–protein gel loading dye (Bio-Rad, Hercules, CA). Following denaturation at 95°C for 10 min, the agarose-bound material was loaded onto a 12% SDS–polyacrylamide gel for electrophoresis, and the protein was stained (except for the PCNA studies, see below) with Sypro Red (Molecular Probes, Invitrogen). Fluorescence was visualized using a Typoon Trio+ Variable Model Imager (Amersham Bioscience/GE Healthcare, Piscataway, NJ), and the signal was quantified using ImageQuant software as detailed by the manufacturer (Molecular Dynamics, GE Healthcare). For the XRCC1-PCNA interaction, western blotting (WB) was performed to detect bound PCNA protein. After affinity capture and SDS–polyacrylamide gel electrophoresis as above, proteins were blotted and detected with either anti-PCNA (rabbit, Santa Cruz, CA, Sc-7907) or anti-XRCC1 (rabbit, GeneTex Inc., Irvine, CA, RB-XRC10-UP50) antibody. A fluorescence-labeled secondary antibody (Alexa Flour 488, anti-rabbit, molecular probes) was used for quantification as above. To quantify binding activity in each of the cases above, background binding seen in the control (no XRCC1, beads only) reaction was first subtracted from the amount of partner protein detected in the different XRCC1 reactions, and then the ratio of partner:XRCC1 was determined. The relative binding activity represents the value obtained by comparing the ratio for the variant XRCC1 protein reaction to the ratio of the WT XRCC1 assay (reported as 100) within a given experimental set.

In the PARP-1-XRCC1 interaction assays, PARP-1 was ADP-ribosylated (unless otherwise indicated). ADP-ribosylation was conducted according to ref. (30), with minor modifications. Eighteen microgram PARP-1 was incubated at 25°C for 20 min in 45 µl reaction buffer [100 mM Tris, pH 8.0, 100 µM NAD^+, 10 mM $MgCl_2$, 5 mM DTT, 34-mer double-stranded DNA (dsDNA) containing a nick (1 pmol/ml)]. Reactions were then stopped by the addition of 1.8 µl 0.5 M EDTA, and aliquots were used accordingly to evaluate the interaction affinity of ADP-ribosylated PARP-1 with the various XRCC1 proteins.

DNA-binding assay

For each set of binding reactions, substrates were prepared in batch. One-hundred and twenty microliter of streptavidin gel matrix solution (Pierce/Thermo Scientific, Rockford, IL) was transferred to a microcentrifuge tube and pelleted by centrifugation at 4500× *g* for 1 min. The matrix was subsequently equilibrated in DNA-binding buffer (1 × PBS, 1% NP-40) by washing three times and resuspending in 800 µl binding buffer. Biotinylated substrate (400 pmol), either gapped DNA (34Gbio/15BER/pG18) or double-stranded undamaged DNA (34Gbio/34C) from Integrated DNA Technology, Coralville, IA or Midland, Midland, TX, were added and incubated at room temperature for 90 min. The streptavadin matrix:biotinylated DNA complex was pelleted, washed twice with DNA-binding buffer, and resuspended in 800 µl binding buffer with BSA (50 µg/ml). Twenty microliter of streptavadin matrix:biotinylated DNA substrate (10 pmol) was aliquoted into individual reaction tubes, and XRCC1 protein (5, 10, 20 or 40 pmol) was added in a final volume of 30 µl. Reactions were incubated overnight at 4°C with rotation to allow for protein:DNA complex formation. The streptavadin matrix:DNA:protein complex was pelleted by centrifugation at 4500× *g* for 1 min and then washed twice with DNA-binding buffer. Any stably bound protein was dissociated from the beads by heating at 95°C for 10 min in SDS–protein loading dye and resolved on a 12% SDS–polyacrylamide gel. Following transfer, WB analysis was performed using primary antibody against XRCC1 (NeoMarkers/Thermo Scientific, 33-2-5). Signals were detected using horseradish peroxidase-conjugated secondary antibodies and SuperSignal West Femto Maximum Sensitivity Substrate (Pierce). WBs were captured as TIFF files and quantitated with ImageQuant TL (GE Biosciences). Nucleic acid saturation binding curves were plotted (% substrate bound versus nM XRCC1 concentration) and apparent dissociation constants were calculated by non-linear curve fitting using the Hill equation in Origin 7.0 (Northampton, MA). For DNA-binding reactions with XRCC1 mutant proteins, 20 pmol of each protein was incubated with 10 pmol of gapped DNA substrate and processed as above. Averages and standard deviations were calculated from at least triplicate experiments and plotted relative to WT XRCC1 binding.

Laser microirradiation and confocal microscopy

We employed a Nikon Eclipse TE2000-E spinning disk confocal microscope with five laser imaging modules and a CCD camera (Hamamatsu, Tokyo, Japan). The set-up integrated a Stanford Research Systems (SRS) NL100 nitrogen laser by Micropoint ablation system (Photonics Instruments, St. Charles, IL), using a 3 ns pulse width at 10 Hz with a diffraction limit spot size of 300 nm. Positions internal to the nucleus of HeLa cells transfected 24 h previously with a YFP-tagged XRCC1 construct (see above) were targeted via a 40× oil objective lens. Transfection was carried out with the FuGENE® 6 Reagent (Roche, Basel, Switzerland) using ~200 000 cells and 1.5 µg plasmid DNA according to the manufacturer's procedure. Site-specific DNA damage was induced using the SRS NL100 nitrogen laser that was passed through a dye cell to emit at 435 nm wavelength. The power of the laser was attenuated through Improvison's Volocity software 4.3.1 (Improvision/PerkinElmer, Coventry, England) in terms of percent intensity. A laser intensity of 1.5% (total energy output of ~10 nW) was used in all experiments to create free radical-induced DNA SSBs in the targeted region; under these parameters, no γH2AX foci, a marker for double-strand breaks, were observed (data not shown). Images were captured at various time points using the same parameters, and the resulting data was analyzed using Volocity version 4.3.1 build 6 (Improvision). Experiments were performed using an environmental chamber attached to the microscope to maintain the normal atmosphere of the cells (i.e. 37°C and 5% CO_2).

Fluorescence recovery after photobleaching analysis

Fluorescence recovery after photobleaching (FRAP) analysis was carried out with live cells transfected with an YFP tagged XRCC1 plasmid as described above. The same set up as the microirradiation was used to perform the photobleaching. Fluorescence recovery was monitored and the data for recovery was corrected for the background intensity and loss of total fluorescence.

RESULTS

Integrity of XRCC1 variant proteins

The various site-specific XRCC1 variant proteins generated for this study were characterized for one of the following reasons (summarized in Table 2): (i) they had been previously shown or argued as disruptive of a specific function and therefore would serve as a control (V86R, in the POLβ interaction; R109A, in the POLβ interaction and/or in DNA binding) (8,9,26); (ii) they were identified as the principal defect responsible for the repair-deficiencies associated with the CHO cell lines EM-C12 and EM-C11 (e.g. E102K and C390Y, respectively, or E98K and C389Y in humans; see protein alignment in Supplementary Figure S1) (24); or (iii) they were found among the normal healthy human population yet may represent impaired-function, disease susceptibility factors (P161L, R194W, R280H, R399Q and Y576S;

Table 2. XRCC1 variant proteins studied here

Variant	Background	Expression efficiency	Purification characteristics
V86R	Impaired POLβ interaction, control protein	Normal	Normal; slightly faster electrophoretic mobility
E98K	Associated with EM-C12 mutant cell line, E102K in CHO; putative DNA-binding mutant	Normal, increased degradation or instability	Normal
R109A	Putative POLβ and DNA-binding mutant	Normal	Normal
P161L	Population variant	Normal	Normal
R194W	Population variant associated with disease susceptibility	Normal	Normal
R280H	Population variant associated with disease susceptibility	Normal	Normal
C389Y	Associated with EM-C11 mutant cell line, C390Y in CHO	Predominantly a protein fragment	See 'Expression efficiency'
R399Q	Population variant associated with disease susceptibility	Normal	Normal
Y576S	Population variant	Normal	Normal

Amino acid change is indicated to left. 'Background' column reveals origin of substitution. Normal = similar to WT protein, with at most a modest deviation. See text for further details.

Table 3. Predicted effects of site-specific XRCC1 amino acid substitutions

Variant	SIFT prediction (Score)	SS element	Solvent accessibility (%)	Tortion angles (φ, ψ)	Overall stability	Tortion	Predicted ΔΔG (kcal/mol)
V86R	Affect protein function (0.04)	Sheet	52.70	−58.7°, 89.4°	Destabilizing	Unfavorable	−0.9
E98K	Affect protein function (0)	Helix	19.46	−65.3°, −24.5°	Destabilizing	Favorable	−3.01
R109A	Affect protein function (0)	Sheet	56.77	−131.9°, 173.8°	Destabilizing	Unfavorable	−0.4
P161L	Tolerated (0.11)	–	–	–	–	–	–
R194W	Tolerated (0.12)	–	–	–	–	–	–
R280H	Tolerated (0.13)	–	–	–	–	–	–
C389Y	Affect protein function (0)	Helix	0.00	−60.8°, −49.5°	Destabilizing	Favorable	−30.7
R399Q	Tolerated (0.19)	Helix	81.22	−67.7°, −21.7°	Destabilizing	Favorable	−6.08
Y576S	Affect protein function (0)	Other	58.49	−168.3°, 146.5°	Stabilizing	Favorable	0.64

Sorting intolerant from tolerant (SIFT) uses sequence homology to predict whether an amino acid substitution will affect protein function (http://blocks.fhcrc.org/sift/SIFT.html). The score is the normalized probability that the amino acid change is tolerated; SIFT predicts substitutions with scores <0.05 as deleterious. CUPSAT is a method based on three-dimensional structural parameters (http://cupsat.tu-bs.de/). This prediction model uses amino acid-atom potentials and torsion angle distribution to assess the amino acid environment of the mutation site. CUPSAT can also distinguish the amino acid environment using its solvent accessibility and secondary-structure specificity. '–' indicates not applicable, as no structure information exits. See Figure 7 legend for further details.

Table 3) (27). Since these amino acid substitutions spanned the length of the XRCC1 protein (Figure 1A), they might represent separation-of-function mutants defective in only a single (or a limited number of) interaction(s).

After expression and purification of the various N-terminal S-peptide-tagged, C-terminal His-tagged, recombinant human XRCC1 proteins, experiments monitoring whether they exhibited an altered or abnormal behavior during the process were conducted (see 'Materials and methods' section for procedure). For the most part, each of the XRCC1 variants acted similar to the WT protein, with V86R and C389Y being the most visible exceptions (Table 2). V86R showed a slight and reproducible altered mobility upon resolution in a 12% SDS–polyacrylamide gel (Tris/glycine-buffered), migrating somewhat faster than the other full-length recombinant XRCC1 fusions (Figure 1B and throughout). C389Y (associated with the mutant CHO cell line EM-C11), both in whole cell extracts (not shown) and following purification via nickel chromatography, was produced largely as an unstable, truncated (presumably degraded) product (Figure 1B). Although not as dramatic as C389Y, the E98K substitution (equivalent to that seen in EM-C12) appears to destabilize the XRCC1 polypeptide as well, as suggested by the increased degradation seen in Figure 1B; E98K also exhibited greater sensitivity than the other proteins to multiple freeze-thaw cycles, as revealed by more rapid degradation (unpublished observation). Other than these deviations, each protein was expressed to a similar degree and with similar solubility, and displayed comparable chromatographic properties as WT XRCC1 (summarized in Table 2). Such data suggest that the particular amino acid change introduced (other than primarily V86R, E98K or C389Y) had little or no major effect on the global structural integrity or general stability of the XRCC1 polypeptide. Additional experimentation was not performed with the C389Y preparation.

To further interrogate the state of the various XRCC1 recombinant proteins, their capacity and efficiency to bind the S-protein affinity matrix was explored. This strategy

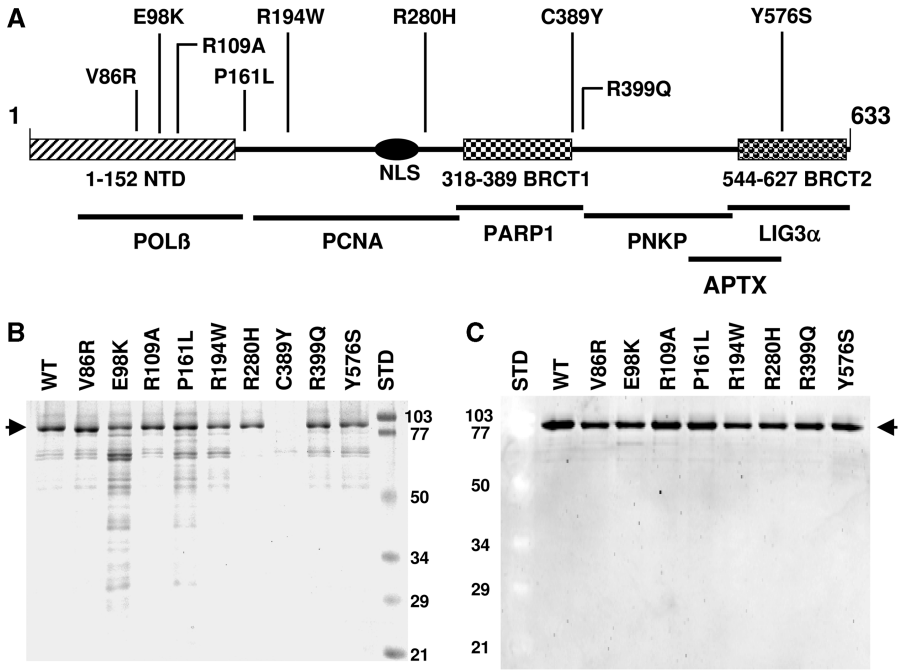

Figure 1. Relevant amino acid positions and regions of human XRCC1, and purification of XRCC1 proteins. (**A**) Linear schematic of the XRCC1 protein. Indicated are the four major conserved elements of XRCC1: the N-terminal domain (NTD), the nuclear localization signals (NLS), the BRCT1 and the BRCT2 domains. Numbers represent the amino acid positions within the XRCC1 polypeptide. The locations of the amino acid substitutions are indicated above the diagram. The regions of XRCC1 that interact with specified protein partners are denoted. (**B**) Nickel column affinity purified XRCC1 proteins. C-terminal His-tagged, N-terminal S-peptide-tagged XRCC1 recombinant proteins expressed in bacteria were purified using nickel chromatography. Shown is an image of the purified proteins separated in a 12% SDS–polyacrylamide gel and stained with coomassie blue. (**C**) Nickel and S-protein affinity purified XRCC1 proteins. Following nickel purification, dual-tagged XRCC1 recombinant proteins were affinity captured using an S-protein matrix. Shown is an image of silver stained purified proteins after separation in a 12% SDS–polyacrylamide gel. Arrows indicate XRCC1. STD = protein standards (in kDa).

was not only an additional means of assessing the integrity of the variant proteins, but also a method to determine sample purity prior to use in the affinity capture (interaction) studies described below. Following binding to the S-protein agarose column, recombinant XRCC1 proteins were eluted, separated on a 12% SDS–polyacrylamide gel, and silver stained. As shown in Figure 1C, all proteins behaved similar to WT (recognizing the exceptions above) and were purified to >95%. The fact that each protein (excluding C389Y) binds to both the nickel and S-protein affinity column indicates that each retains the C- and N-terminal hexahistidine and S-peptide tags, respectively, and therefore is full-length. This observation suggests that the apparent slightly altered electrophoretic mobility of recombinant V86R arises from a unique physical or chemical feature induced by the amino acid change, and not an N- or C-terminal truncation.

Interaction affinities of XRCC1 proteins

We examined the interaction stability of the various XRCC1 variants with several major associating protein partners (Figure 1A). Towards this end, a previously devised affinity capture strategy was employed (14). This approach involved binding of the S-peptide-tag recombinant fusion proteins to the S-protein agarose matrix (Figure 1C), and subsequently incubating this complex with a protein of interest. After permitting the protein–protein interaction to occur (at a concentration of protein determined to be within the linear range of binding; see for instance, Figure 2A), bound material was captured, separated on a denaturing SDS–polyacrylamide gel, and either stained with Sypro Red or visualized via WB analysis using fluorescence-labeled secondary antibody. Both approaches permitted reliable quantification of the signal intensity of the relevant bands (see 'Materials and Methods' section). The amount of retained target protein relative to XRCC1 was plotted against the value obtained for WT (arbitrarily set at 100), with reduced retention indicating impaired interaction stability.

Initial studies examined the effect of the various amino acid substitutions on the association of XRCC1 with DNA POLβ (Figure 2). As anticipated, the most dramatic effect was observed with the V86R mutant, where POLβ retention was equivalent to (or less than) the POLβ alone (beads only) negative control in three independent experimental runs (Figure 2B and C). This is in line with prior biochemical experiments using the N-terminal domain (NTD) of XRCC1 (26) and with yeast two-hybrid analysis using the full-length protein (8), where both studies indicated that a V to R substitution at position 86 profoundly destabilized the POLβ interaction, validating the experimental *in vitro* approach. In addition, we observed a reproducible and significant ~5-fold (83%) decrease in POLβ retention with the R109A variant (Figure 2B and C), a finding also consistent with prior biochemical studies using an N-terminal

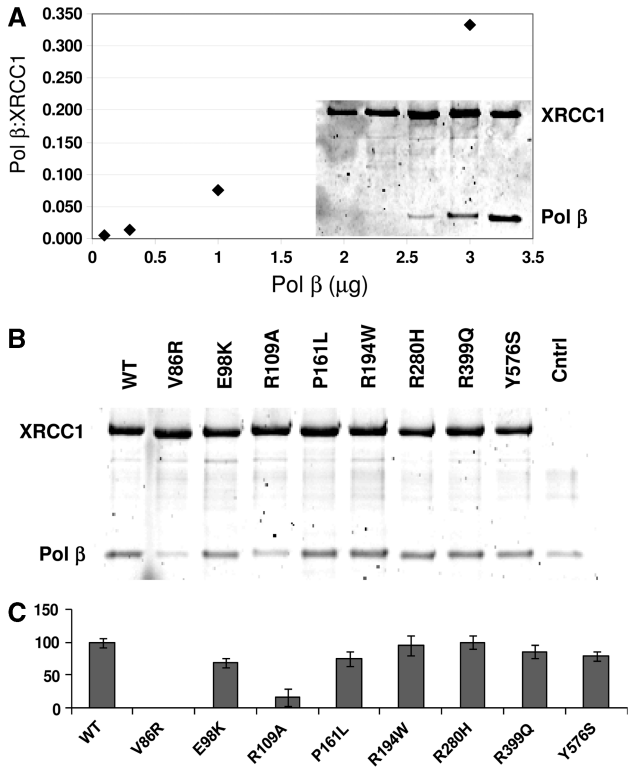

Figure 2. Interaction of XRCC1 with DNA POLβ. (**A**) Titration of XRCC1–POLβ interaction. XRCC1 (4 μg) was bound to S-protein agarose, mixed with POLβ (0.1, 0.3, 1 or 3 μg), and the two proteins captured as described in 'Materials and Methods' section. Bound proteins were separated in a 12% SDS–polyacrylamide gel and stained with Sypro Red (inset). The resulting signal ratio of POLβ/XRCC1 (*y*-axis) is plotted against the initial POLβ amount (*x*-axis). (**B**) A representative gel image of an XRCC1–POLβ affinity capture experiment. Experiment was carried out with the indicated XRCC1 protein (4 μg) and POLβ (2 μg). The intensity of the minor (background) POLβ band seen in the V86R lane was similar to the negative control reaction without XRCC1 (i.e. POLβ alone, Cntrl). (**C**) Relative interaction affinity of XRCC1 proteins for POLβ. Shown is the average and standard deviation of three independent experimental runs. Values represent the POLβ:XRCC1 signal ratio, with WT being arbitrarily set at 100. Standard deviation of the values for the WT-binding reactions is shown as well.

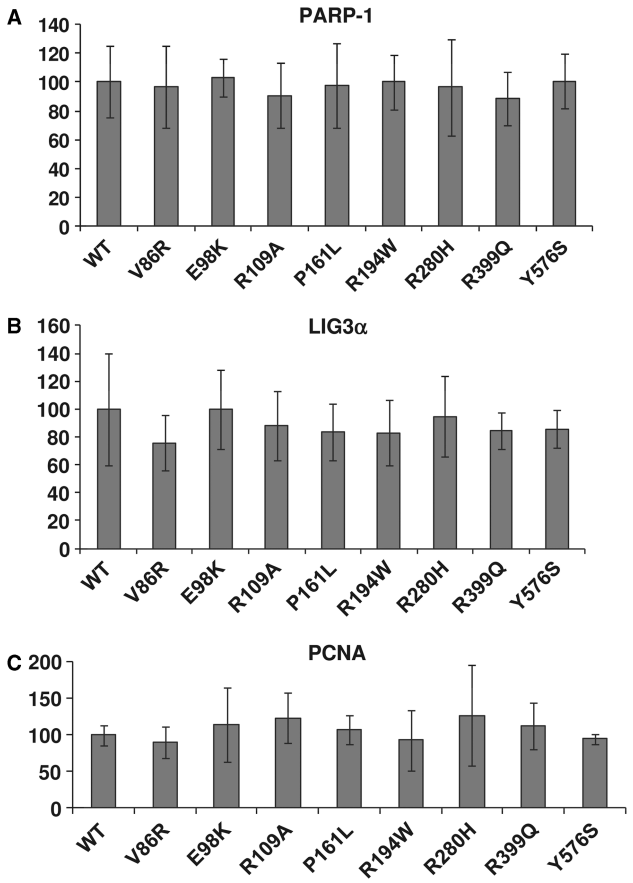

Figure 3. Relative affinities of XRCC1 proteins for PARP-1 (**A**), LIG3α (**B**) and PCNA (**C**). Shown are the average and standard deviation of three independent affinity capture experiments. See Figure 2, as well as text, for further details. Values represent the resulting signal ratio, with WT being arbitrarily set to 100. Standard deviation of the values for the WT-binding reactions is shown as well.

XRCC1 fragment containing a R109S substitution (26). No defect (i.e. <20%) in the POLβ interaction was seen for the XRCC1 variants R194W, R280H and R399Q, whereas a marginal defect (~20–30%) was observed for Y576S, as well as with E98K and P161L (Figure 2B and C), the latter two of which harbor an amino acid change within or near the POLβ interaction domain (Figure 1A).

As the above experiments with DNA POLβ validated the use of the affinity capture technique to assess relative binding affinity [see for instance, ref. (26)], similar interaction studies using the purified protein partners PARP-1, LIG3α and PCNA, which span the various functional regions of the XRCC1 polypeptide, were performed (Figure 1A). As shown in Figure 3A, ADP-ribosylated PARP-1 interacted with all of the XRCC1 variant proteins with similar affinity as WT. We note that ADP-ribosylation of PARP-1 enhanced the interaction with WT XRCC1 (Supplementary Figure S2), as described previously (7,33). As with PARP-1, no interaction deficiency for any of the XRCC1 variants was observed with DNA LIG3α (Figure 3B). Given that the association of XRCC1 with PCNA appears 5-fold weaker than its association with the other proteins examined herein, we used WB analysis to improve the detection of captured PCNA. These studies revealed that none of the variant XRCC1 proteins exhibited a statistically significant defect in their affinity for PCNA (Figure 3C).

DNA-binding activities of XRCC1 proteins

Besides the specific protein–protein interactions outlined in Figure 1A, XRCC1 has also been reported to exhibit nick- or gap-preferred DNA-binding activity (25,34). In addition, the BRCT2 domain of XRCC1 has been shown to associate with DNA double-strand break ends (35). Studies were designed to determine the impact of the various site-specific mutations on DNA binding. Towards this end, an affinity matrix DNA-binding assay was developed. In brief,

single-stranded 34-mer 5′-biotin-tagged oligonucleotide (34Gbio) and complementary oligonucleotides (34C, 34F or 15BER/pG18) were annealed to create unmodified (dsDNA) or damage-containing (either AP-DNA or Gap DNA) substrate molecules (Supplementary Figure S3A). These DNA molecules were affixed to streptavidin agarose beads and subsequently incubated with the protein of interest (see below) to permit complex assembly, washed to remove unbound or weakly bound material, and then analyzed by WB to reveal the presence of stably bound protein. The more stable the interaction, the more protein that will be retained on the DNA matrix.

To establish the utility of this approach, Ape1 binding to unmodified duplex DNA and duplex DNA containing an AP site (AP-DNA) at various substrate concentrations was examined. We anticipated that more Ape1 protein would be associated with AP-DNA than with unmodified duplex DNA, based on previously-determined affinities (36). As shown in Supplementary Figure S3B (upper panel), a significant difference between the signal for the AP duplex and the normal duplex (~4-fold) when 20 pmol DNA and 2.8 pmol Ape1 were used. An additional means of method validation, DNA POLβ, the major gap-filling DNA polymerase in mammals, was also employed (37). As shown in Supplementary Figure S3B (lower panel), at each concentration of DNA tested, POLβ exhibited a more stable interaction with the 1-nt gap substrate relative to the unmodified dsDNA control, consistent with the reported data (38) and similar to what was anticipated for XRCC1 (see below). These studies indicate that such a binding approach can be employed to reveal DNA-binding preferences, at least semi-quantitatively.

Using parameters established above and dsDNA and Gap DNA (Supplementary Figure S3A), the comparative binding affinities of WT XRCC1 were determined. Such analysis indicated that under the conditions used herein, XRCC1 binds the two 34-mer oligonucleotide substrates with similar affinities (apparent K_D values of ~600 nM) (Figure 4A and B). Since previous studies have indicated a higher affinity for nick and gapped DNA substrates relative to intact duplex DNAs (25,34), the utility of the assay was re-evaluated by examining binding of the NTD of XRCC1 ($XRCC1_{NTD}$) to dsDNA and Gap DNA. Consistent with the previous reports, $XRCC1_{NTD}$ preferentially bound to Gap DNA relative to dsDNA, with ~2-fold preference in these assay conditions (Supplementary Figure S3C).

Finally, the DNA-binding affinities of the variant XRCC1 proteins for Gap DNA were compared. These studies revealed that V86R (1.5-fold), E98K (1.7-fold), R109A (1.5-fold) and R194W (1.5-fold) displayed slightly enhanced affinities for the Gap DNA duplex substrate in comparison to WT XRCC1 (Figure 4C). Interestingly, the R280H mutant displayed a decreased affinity for Gap DNA binding relative to WT. None of the other variants exhibited a quantitative difference in DNA-binding affinity for dsDNA containing a 1-nt gap (Figure 4C).

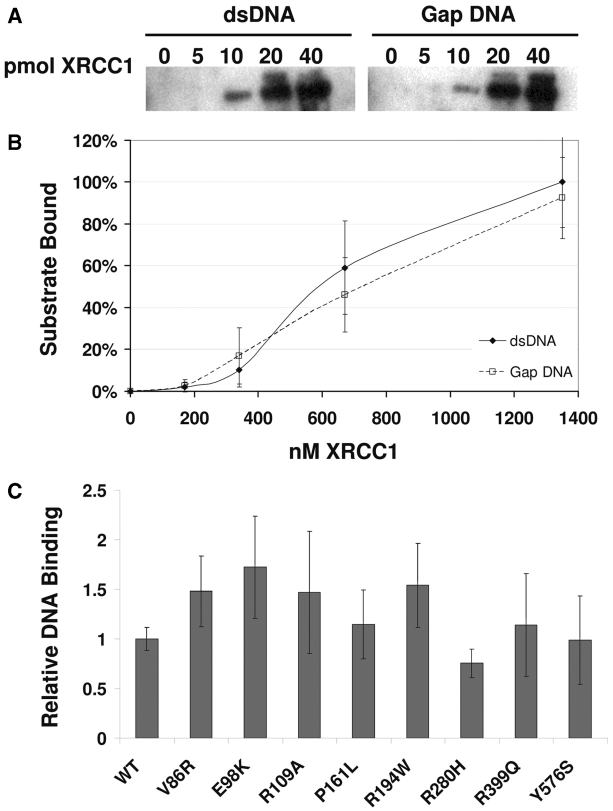

Figure 4. Binding of XRCC1 to DNA. (**A**) Representative WB blot. Indicated substrates (10 pmol) were captured on streptavidin beads and incubated with XRCC1 (5, 10, 20 or 40 pmol), and bound protein was pulled down and detected by WB. (**B**) Graph displaying full-length XRCC1 binding to unmodified duplex or single nucleotide gapped DNA substrates. Shown is the average and standard deviation of three independent experimental runs. (**C**) DNA-binding activities of the XRCC1 variants. Shown is a graph of the binding to Gap DNA of various XRCC1 mutant proteins compared to WT. Standard deviation of the values for the WT XRCC1 binding reactions is shown as well.

Intracellular localization and distribution dynamics of XRCC1 proteins

YFP-tagged XRCC1 expression constructs, for each of the variants outlined in Table 2, were created to determine protein localization and functional capacity in human cells. Specifically, the intracellular localization and the damage-induced redistribution kinetics of each XRCC1 protein after transient transfection into HeLa cells were evaluated. As shown in Figure 5, under normal cell culture conditions, other than mutant E98K, each of the XRCC1 variants appeared similar to WT in that the protein resided largely in the nucleoplasm, exhibiting in some instances a punctated foci pattern that was found previously to reflect S-phase cells and active replication factories (e.g. see WT, inset) (14), and was excluded from the nucleolus. C389Y, although showing a sub-cellular distribution similar to WT, exhibited a reduced fluorescent signal intensity in many of the cells (Figure 5, solid arrow heads), likely indicative of the protein instability observed in bacteria (Figure 1). As for E98K, this mutant displayed an irregular distribution pattern in which the protein was

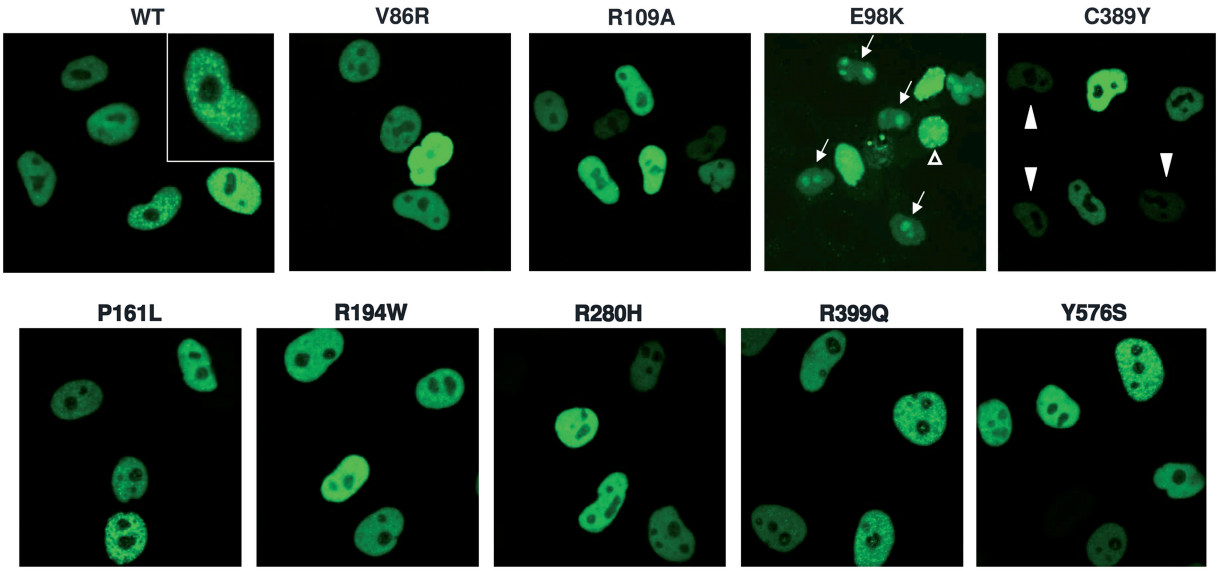

Figure 5. Intracellular distribution of XRCC1 variants. The indicated XRCC1 YFP-tagged fusion protein constructs were transiently transfected into HeLa cells, and fluorescent protein visualized by 491 nm GFP laser. The inset highlights a WT expressing cell with punctated nuclear staining. The arrows indicate cells where E98K is concentrated in the nucleolus, while the open arrow head denotes a cell with broad nuclear staining and strong punctated foci. The closed arrow heads point out cells that express C389Y at low levels.

sequestered primarily in the nucleolus in most cells (Figure 5, arrows), although in some instances, the mutant exhibited sharp punctated staining in the nucleoplasm (Figure 5, open arrow head).

Since XRCC1 interacts with several protein partners during the response to DNA SSBs (6), we reasoned that examination of the relocalization kinetics of the XRCC1 variants would uncover any deleterious effect of a particular amino acid substitution on protein coordination events that take place *in vivo*. Specifically, the redistribution dynamics of the XRCC1 variants to/from site-specifically, laser-induced DNA damage under parameters that generated DNA single-, but not double-strand breaks, were determined (see 'Materials and methods' section). For relocalization to the sites of DNA damage, each of the variant proteins displayed WT kinetics, appearing at the laser-targeted region ~10–15 s (Supplementary Figure S4), except for E98K, which never formed observable stripes (data not shown), presumably due to its abnormal localization pattern (Figure 5), and C389Y, which also never formed detectable stripes (Figure 6A), likely due to its reduced protein stability and possibly as a consequence of a defective interaction with PARP-1 (see site of substitution in Figure 1A).

Disappearance of the YFP-XRCC1 signal was also monitored from the site of laser-induced DNA SSBs. As shown in Supplementary Figure S5, each of the XRCC1 variants displayed retention kinetics similar to WT, with stripe dissolution occurring from ~45 min to 1 h after damage induction; E98K and C389Y were not evaluated in these experiments as they did not localize to the site of DNA damage (see above). The lone exception to this result was the R280H polymorphic variant, which exhibited slightly reduced retention kinetics, disappearing ~15–30 min post-microirradiation (Figure 6B).

DISCUSSION

XRCC1 is a non-enzymatic scaffold protein thought to coordinate and facilitate efficient SSBR through its numerous protein-protein interactions (6). Complete absence of XRCC1 in mice leads to embryonic lethality, and a deficiency in this protein in mammalian cells results in chromosome instability and increased DNA-damaging agent sensitivity (39–42). Furthermore, XRCC1 has been linked to proteins found to be defective in inherited spinocerebellar ataxias, e.g. TDP1 and Aprataxin, suggesting a connection between SSBR efficiency and neuronal cell survival (43,44). Given this information, it seems reasonable to hypothesize that individuals with impaired XRCC1 function would exhibit elevated risk of disease manifestation. These studies were aimed to define the functional capacities of XRCC1 variants found in repair-deficient CHO cell lines as well as in the human population (Tables 2 and 3).

The structure-based V86R mutation completely disrupts the interaction of XRCC1 with DNA POLβ *in vitro* [consistent with previous findings (8,26)], but this substitution does not affect binding to PCNA, PARP-1, or LIG3α. Molecular modeling of the V86R mutation reveals a significant change in the electrostatic charge of the NTD of XRCC1, whereby the largely negatively charged interface of the WT protein becomes mainly positive in the mutant (Figure 7A). This change in electrostatic surface charge likely is the reason for the decreased POLβ binding. Given the findings within, V86R appears to represent a true, separation-of-function mutant. Studies demonstrating the inability of V86R to complement the repair-deficiencies of *xrcc1* mutant CHO cell lines (8,9) highlight the importance of the XRCC1–POLβ interaction in mediating a proficient DNA damage response. However, the localization studies in HeLa cells indicate that interaction between these two proteins is not critical

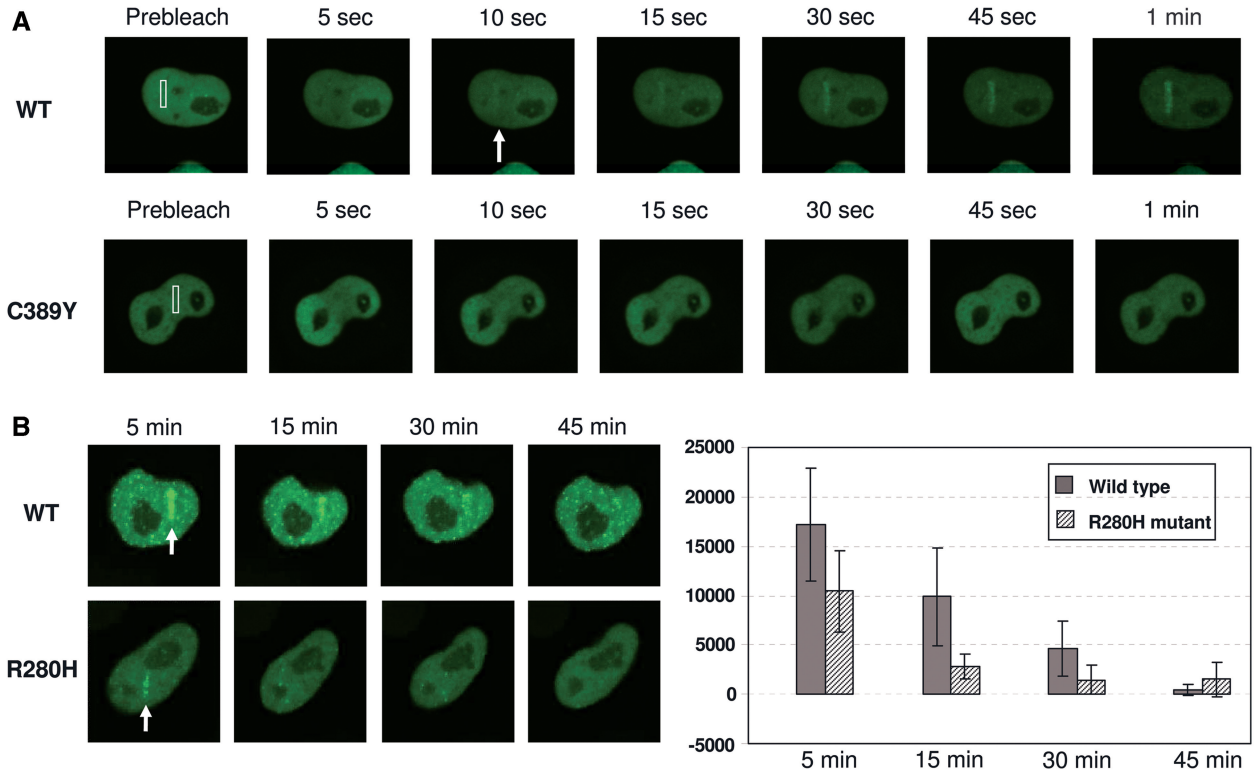

Figure 6. Relocalization of XRCC1 proteins to and from sites of laser-induced DNA damage. (**A**) Redistribution kinetics of WT and the XRCC1 C389Y variant. Shown are still images taken at the indicated time point (in seconds) after prebleach. The box denotes the region of laser-induced DNA damage, while the arrow indicates the first point and location at which clear 'stripe' formation is observed. (**B**) Retention kinetics of WT and R280H XRCC1 proteins. After laser-induced DNA damage induction, peak stripe was observed at 5 min. Shown is the loss of signal at 15, 30 and 45 min post-irradiation. Each protein (denoted) was analyzed five times and the data presented are mean intensity values obtained in a given experiment following of substraction of the prebleach background.

for targeting XRCC1 to laser-induced DNA damage, which is presumably comprised of primarily free radical-generated SSBs. This protein–protein interaction may instead be required to facilitate POLβ gap-filling polymerization activity (45) and/or coordinate efficient nick ligation (46), although normal disassembly of V86R XRCC1 stripes from sites of introduced DNA damage was seen.

In vitro studies revealed that the structure/function-based R109A substitution results in a ~80% reduced binding affinity of XRCC1 for full-length DNA POLβ. This observation is consistent with the prediction that R109 mediates interactions with POLβ (Figure 7A) and with biochemical data indicating that an R109S substitution in the NTD of XRCC1 reduces (by ~30-fold) binding affinity for the 22 kDa interaction domain of POLβ (25,26). Interestingly, the R109A mutant displayed normal DNA-binding activity, arguing against a prominent role for this residue in directing protein–DNA interactions as suggested previously. In line with the results of V86R, normal relocalization kinetics for the R109A mutant in the laser-induced DNA damage response studies were observed, supporting the conclusion that the physical association of XRCC1 with POLβ is not essential for effective targeting of the former protein to sites of DNA damage.

The XRCC1 mutants C389Y and E98K, which are responsible for the repair deficiencies of the EM-C11 and EM-C12 CHO cell lines, respectively, were found to exhibit varying degrees of expression efficiency/stability when produced in bacteria. In the case of C389Y, little to no full-length protein was detected in bacterial cell lysates or following nickel-column chromatography. This impaired protein production/stability is consistent with the absence of C389Y in EM-C11 cell extracts as determined by WB analysis (24), and suggests that the CHO EM-C11 mutant line is for all extensive purposes XRCC1 null. Amino acid position 389 is buried within the XRCC1 protein structure and is predicted to have no solvent accessibility, and both sorting intolerant from tolerant (SIFT) and Cologne university protein stability analysis tool (CUPSAT) calculate that a C389Y mutation would destabilize or adversely affect protein function (Table 3). That said, WT expression of C389Y was observed in a subset of HeLa cells. In situations where C389Y was detectable, the mutant protein was not targeted to sites of laser-induced DNA damage. Since this residue is positioned within the PARP-1 interaction domain, it is possible that this amino acid change negatively affects this protein–protein association, resulting in impaired recruitment of XRCC1 to sites of lesion processing. Indeed, prior studies have demonstrated that XRCC1 targeting and function is dependent on poly(ADP-ribosyl)ation and PARP-1 at DNA SSBs (47–49).

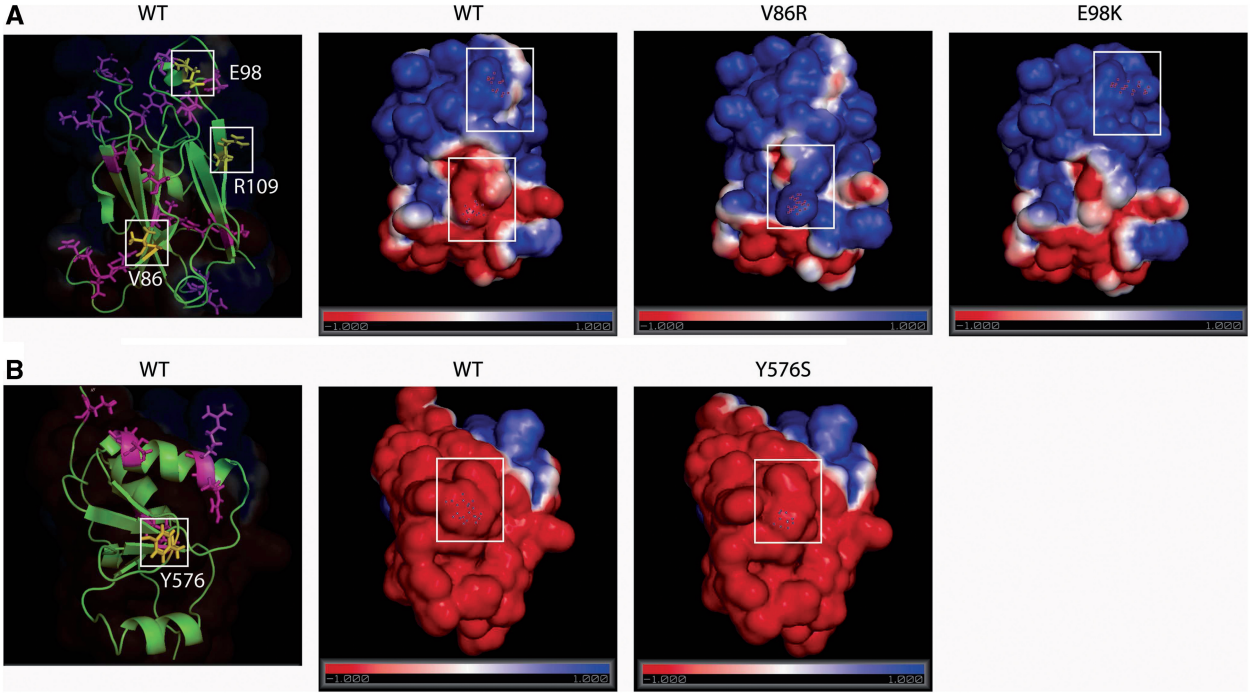

Figure 7. Molecular modeling of XRCC1 and site-specific mutants. XRCC1 N-terminus (PDB ID: 1XNA), BRCT1 (PDB ID: 2D8M) and BRCT2 (PDB ID: 1CDZ) domains were downloaded from PDB (http://www.rcsb.org/pdb). Variant structure models were generated using SWISS-MODEL (http://swissmodel.expasy.org//SWISS-MODEL.html). Electrostatic surface charge calculations were generated by creating PQR files using PDB2PQR (http://pdb2pqr.sourceforge.net/), and subsequently the biomolecular solvation was modeled through solution of the Poisson-Boltzman equation by APBS (http://apbs.sourceforge.net/) and visualized using PyMol (DeLano Scientific). (**A**) WT XRCC1 NTD displaying POLβ interacting amino acids (magenta) and positions of disruptive amino acid mutants (yellow) boxed in white (left panel). Electrostatic surface charge models of XRCC1 N-terminus for WT, V86R and E98K. White boxes denote amino acid position 86 or 98, as essentially arranged in panel to left, and the immediately surrounding amino acids. (**B**) WT XRCC1 C-terminal BRCT domain displaying Ligase III interacting amino acids (magenta) and position of non-disruptive amino acid position 576 (yellow) boxed in white (left panel). Electrostatic surface charge models of XRCC1 C-terminal BRCT domain WT and Y576S. White boxes denote amino acid position 576 and immediately surrounding amino acids.

In the case of E98K, the recombinant protein exhibited only a slight decrease in overall stability when expressed in bacteria as revealed by increased degradation (although the protein did show hypersensitivity to freeze-thaw events). This is in apparent contrast to the observation that E98K is absent from EM-C12 cell extracts (24), but may reflect differences in expression conditions and/or cellular environments, variation in half-life stability, limitations in WB detection, or stabilization by the affinity or visualization tags. Nonetheless, the biochemical data herein suggest that the cellular defects associated with EM-C12 are likely the cumulative result of (i) reduced XRCC1 protein levels (24), (ii) a slightly impaired interaction with DNA POLβ and (iii) a slightly enhanced DNA-binding affinity, a feature that is consistent with the previous proposal that mutation of E98 to a positively charged residue such as K might enhance DNA-binding affinity (25). Molecular modeling of the electrostatic surface of E98K predicted an increase in positive charge compared to WT XRCC1 (Figure 7A), a change that likely affects interactions with both POLβ and DNA. Finally, the studies performed in HeLa cells revealed an unusual localization pattern for E98K, where the protein was found primarily sequestered in the nucleolus. In fact, the laser-mediated redistribution experiments did not detect relocalization of E98K to the sites of DNA damage (data not shown), presumably the result of abnormal XRCC1 intracellular targeting.

Our data indicate that full-length XRCC1 exhibits similar DNA-binding activity for unmodified duplex DNA and duplex DNA containing a single nucleotide gap. Previous studies, however, have found that XRCC1 displays a higher affinity for DNA containing a nick (~7–8-fold) or a one nucleotide gap (~3–4-fold) than for intact ds or ssDNA (34). Since we demonstrated that $XRCC1_{NTD}$ exhibits increased binding activity for Gap DNA relative to dsDNA (Supplementary Figure S3C), our results suggest that additional portions of XRCC1 likely contribute to DNA binding, such as the BRCT2 domain (35). Supportive of this, slightly enhanced Gap DNA binding for the R194W variant and decreased binding for R280H, residues that fall outside of the NTD of XRCC1, was observed (Figure 1A). It seems worthwhile to more thoroughly define the molecular nature of the XRCC1–DNA interaction(s), as well as the contributions of the various protein domains to substrate recognition/discrimination.

Neither of the rare variants, P161L or Y576S (found at frequencies of ≤1% in the human population), were found *in vitro* to exhibit major defects in their interaction affinities with POLβ, PCNA, PARP-1, LIG3α or DNA. While there was some indication that P161L may display a

marginal defect in its interaction with POLβ, this ~20% deficiency likely reflects limitations in the assay, as a similar defect was seen for Y576S, a mutation some distance from the POLβ interacting region (Figure 1A). The lack of an interaction defect between Y576S and DNA LIG3α is consistent with (i) this amino acid residue location in XRCC1 is somewhat distant from the precise protein-protein interface (Figure 7B) and (ii) a mutation that does not dramatically affect surface electrostatic charge (Figure 7B) or protein structural integrity as assessed by CUPSAT (Table 3). Since P161L and Y576S are similar in function to the WT protein, including in their cellular localization patterns, it is unlikely that either is a susceptibility or disease allele.

As for the high frequency (polymorphic) variants, R194W and R399Q, no major interaction deficiency was observed for the primary protein partners POLβ, PCNA, PARP-1 and LIG3α, or for DNA. Moreover, these variants, as well as R280H, exhibited normal intracellular distribution patterns when expressed in HeLa cells, indicating no impairment, for instance, of the putative nuclear localization signal. While several reports have described an association of R194W or R399Q with disease susceptibility (21,50,51), there are nearly as many studies that have failed to see a risk association for these variants. Since none of the studies herein indicate that R194W and R399Q XRCC1 proteins are functionally defective, it seems unlikely that they are responsible for the investigated disease development. As for R280H, this variant displayed a shortened retention time at sites of laser-induced DNA SSBs, as well as a slight defect in DNA binding *in vitro*. Such results are seemingly consistent with past complementation experiments, in which two out of three studies have found that R280H exhibits an impaired biological function (52–54). Moreover, a few investigations have found that the R280H variant of XRCC1, in contrast to variants R194W or R399Q, imparts a reduced DNA repair capacity phenotype as assessed by the Comet assay (55,56). Thus, although there are mixed reports on R280H, our data supports the evidence that the R280H genotype is more likely a negative risk factor than R194W and R399Q in disease susceptibility, possibly due to a defect in DNA binding.

SUPPLEMENTARY DATA

Supplementary Data are available at NAR Online.

ACKNOWLEDGEMENTS

The authors thank Dr Parameswary Muniandy and Dr Scott Maynard (NIA) for their helpful comments.

FUNDNG

Funding for open access charge: Intramural Research Program, National Institute on Aging, National Institutes of Health; National Institute on Aging; (ES12512 and CA92584 to A.E.T.).

Conflict of interest statement. None declared.

REFERENCES

1. Lindahl,T. (1993) Instability and decay of the primary structure of DNA. *Nature*, **362**, 709–715.
2. Hoeijmakers,J.H. (2001) Genome maintenance mechanisms for preventing cancer. *Nature*, **411**, 366–374.
3. Kulkarni,A. and Wilson,D.M. III (2008) The involvement of DNA-damage and -repair defects in neurological dysfunction. *Am. J. Hum. Genet.*, **82**, 539–566.
4. Lombard,D.B., Chua,K.F., Mostoslavsky,R., Franco,S., Gostissa,M. and Alt,F.W. (2005) DNA repair, genome stability, and aging. *Cell*, **120**, 497–512.
5. Wilson,D.M. III and Bohr,V.A. (2007) The mechanics of base excision repair, and its relationship to aging and disease. *DNA Repair (Amst)*, **6**, 544–559.
6. Caldecott,K.W. (2003) XRCC1 and DNA strand break repair. *DNA Repair (Amst)*, **2**, 955–969.
7. Masson,M., Niedergang,C., Schreiber,V., Muller,S., Menissier-de Murcia,J. and de Murcia,G. (1998) XRCC1 is specifically associated with poly(ADP-ribose) polymerase and negatively regulates its activity following DNA damage. *Mol. Cell Biol.*, **18**, 3563–3571.
8. Dianova,I.I., Sleeth,K.M., Allinson,S.L., Parsons,J.L., Breslin,C., Caldecott,K.W. and Dianov,G.L. (2004) XRCC1-DNA polymerase beta interaction is required for efficient base excision repair. *Nucleic Acids Res.*, **32**, 2550–2555.
9. Wong,H.K. and Wilson,D.M. III (2005) XRCC1 and DNA polymerase beta interaction contributes to cellular alkylating-agent resistance and single-strand break repair. *J. Cell Biochem.*, **95**, 794–804.
10. Whitehouse,C.J., Taylor,R.M., Thistlethwaite,A., Zhang,H., Karimi-Busheri,F., Lasko,D.D., Weinfeld,M. and Caldecott,K.W. (2001) XRCC1 stimulates human polynucleotide kinase activity at damaged DNA termini and accelerates DNA single-strand break repair. *Cell*, **104**, 107–117.
11. Caldecott,K.W., McKeown,C.K., Tucker,J.D., Ljungquist,S. and Thompson,L.H. (1994) An interaction between the mammalian DNA repair protein XRCC1 and DNA ligase III. *Mol. Cell Biol.*, **14**, 68–76.
12. Taylor,R.M., Moore,D.J., Whitehouse,J., Johnson,P. and Caldecott,K.W. (2000) A cell cycle-specific requirement for the XRCC1 BRCT II domain during mammalian DNA strand break repair. *Mol. Cell Biol.*, **20**, 735–740.
13. Moore,D.J., Taylor,R.M., Clements,P. and Caldecott,K.W. (2000) Mutation of a BRCT domain selectively disrupts DNA single-strand break repair in noncycling Chinese hamster ovary cells. *Proc. Natl Acad. Sci. USA*, **97**, 13649–13654.
14. Fan,J., Otterlei,M., Wong,H.K., Tomkinson,A.E. and Wilson,D.M. III (2004) XRCC1 co-localizes and physically interacts with PCNA. *Nucleic Acids Res.*, **32**, 2193–2201.
15. Parlanti,E., Locatelli,G., Maga,G. and Dogliotti,E. (2007) Human base excision repair complex is physically associated to DNA replication and cell cycle regulatory proteins. *Nucleic Acids Res.*, **35**, 1569–1577.
16. Levy,N., Oehlmann,M., Delalande,F., Nasheuer,H.P., Van,D.A., Schreiber,V., de,M.G., Menissier-de,M.J., Maiorano,D. and Bresson,A. (2009) XRCC1 interacts with the p58 subunit of DNA Pol alpha-primase and may coordinate DNA repair and replication during S phase. *Nucleic Acids Res.*, **37**, 3177–3188.
17. Thompson,L.H. and West,M.G. (2000) XRCC1 keeps DNA from getting stranded. *Mutat. Res.*, **459**, 1–18.
18. Cheadle,J.P. and Sampson,J.R. (2003) Exposing the MYtH about base excision repair and human inherited disease. *Hum. Mol. Genet.*, **12(Spec No 2)**, R159–R165.
19. Hagen,L., Pena-Diaz,J., Kavli,B., Otterlei,M., Slupphaug,G. and Krokan,H.E. (2006) Genomic uracil and human disease. *Exp. Cell Res.*, **312**, 2666–2672.
20. Sweasy,J.B., Lang,T. and Dimaio,D. (2006) Is base excision repair a tumor suppressor mechanism? *Cell Cycle*, **5**, 250–259.
21. Ladiges,W.C. (2006) Mouse models of XRCC1 DNA repair polymorphisms and cancer. *Oncogene*, **25**, 1612–1619.

22. Tudek,B. (2007) Base excision repair modulation as a risk factor for human cancers. *Mol. Aspects Med.*, **28**, 258–275.
23. Maynard,S., Schurman,S.H., Harboe,C., de Souza-Pinto,N.C. and Bohr,V.A. (2009) Base excision repair of oxidative DNA damage and association with cancer and aging. *Carcinogenesis*, **30**, 2–10.
24. Shen,M.R., Zdzienicka,M.Z., Mohrenweiser,H., Thompson,L.H. and Thelen,M.P. (1998) Mutations in hamster single-strand break repair gene XRCC1 causing defective DNA repair. *Nucleic Acids Res.*, **26**, 1032–1037.
25. Marintchev,A., Mullen,M.A., Maciejewski,M.W., Pan,B., Gryk,M.R. and Mullen,G.P. (1999) Solution structure of the single-strand break repair protein XRCC1 N-terminal domain. *Nat. Struct. Biol.*, **6**, 884–893.
26. Marintchev,A., Gryk,M.R. and Mullen,G.P. (2003) Site-directed mutagenesis analysis of the structural interaction of the single-strand-break repair protein, X-ray cross-complementing group 1, with DNA polymerase beta. *Nucleic Acids Res.*, **31**, 580–588.
27. Mohrenweiser,H.W., Xi,T., Vazquez-Matias,J. and Jones,I.M. (2002) Identification of 127 amino acid substitution variants in screening 37 DNA repair genes in humans. *Cancer Epidemiol. Biomarkers Prev.*, **11**, 1054–1064.
28. Erzberger,J.P. and Wilson,D.M. III (1999) The role of Mg2+ and specific amino acid residues in the catalytic reaction of the major human abasic endonuclease: new insights from EDTA-resistant incision of acyclic abasic site analogs and site-directed mutagenesis. *J. Mol. Biol.*, **290**, 447–457.
29. Nguyen,L.H., Barsky,D., Erzberger,J.P. and Wilson,D.M. III (2000) Mapping the protein-DNA interface and the metal-binding site of the major human apurinic/apyrimidinic endonuclease. *J. Mol. Biol.*, **298**, 447–459.
30. Marsischky,G.T., Wilson,B.A. and Collier,R.J. (1995) Role of glutamic acid 988 of human poly-ADP-ribose polymerase in polymer formation. Evidence for active site similarities to the ADP-ribosylating toxins. *J. Biol. Chem.*, **270**, 3247–3254.
31. Levin,D.S., Bai,W., Yao,N., O'Donnell,M. and Tomkinson,A.E. (1997) An interaction between DNA ligase I and proliferating cell nuclear antigen: implications for Okazaki fragment synthesis and joining. *Proc. Natl Acad. Sci. USA*, **94**, 12863–12868.
32. Mackey,Z.B., Ramos,W., Levin,D.S., Walter,C.A., McCarrey,J.R. and Tomkinson,A.E. (1997) An alternative splicing event which occurs in mouse pachytene spermatocytes generates a form of DNA ligase III with distinct biochemical properties that may function in meiotic recombination. *Mol. Cell Biol.*, **17**, 989–998.
33. Schreiber,V., Ame,J.C., Dolle,P., Schultz,I., Rinaldi,B., Fraulob,V., Menissier-de Murcia,J. and de Murcia,G. (2002) Poly(ADP-ribose) polymerase-2 (PARP-2) is required for efficient base excision DNA repair in association with PARP-1 and XRCC1. *J. Biol. Chem.*, **277**, 23028–23036.
34. Mani,R.S., Karimi-Busheri,F., Fanta,M., Caldecott,K.W., Cass,C.E. and Weinfeld,M. (2004) Biophysical characterization of human XRCC1 and its binding to damaged and undamaged DNA. *Biochemistry*, **43**, 16505–16514.
35. Yamane,K., Katayama,E. and Tsuruo,T. (2000) The BRCT regions of tumor suppressor BRCA1 and of XRCC1 show DNA end binding activity with a multimerizing feature. *Biochem. Biophys. Res. Commun.*, **279**, 678–684.
36. Wilson,D.M. III, Takeshita,M. and Demple,B. (1997) Abasic site binding by the human apurinic endonuclease, Ape, and determination of the DNA contact sites. *Nucleic Acids Res.*, **25**, 933–939.
37. Wilson,S.H. (1998) Mammalian base excision repair and DNA polymerase beta. *Mutat. Res.*, **407**, 203–215.
38. Prasad,R., Beard,W.A. and Wilson,S.H. (1994) Studies of gapped DNA substrate binding by mammalian DNA polymerase beta. Dependence on 5′-phosphate group. *J. Biol. Chem.*, **269**, 18096–18101.
39. Tebbs,R.S., Flannery,M.L., Meneses,J.J., Hartmann,A., Tucker,J.D., Thompson,L.H., Cleaver,J.E. and Pedersen,R.A. (1999) Requirement for the Xrcc1 DNA base excision repair gene during early mouse development. *Dev. Biol.*, **208**, 513–529.
40. Thompson,L.H., Brookman,K.W., Jones,N.J., Allen,S.A. and Carrano,A.V. (1990) Molecular cloning of the human XRCC1 gene, which corrects defective DNA strand break repair and sister chromatid exchange. *Mol. Cell Biol.*, **10**, 6160–6171.
41. Brem,R. and Hall,J. (2005) XRCC1 is required for DNA single-strand break repair in human cells. *Nucleic Acids Res.*, **33**, 2512–2520.
42. Kulkarni,A., McNeill,D.R., Gleichmann,M., Mattson,M.P. and Wilson,D.M. III (2008) XRCC1 protects against the lethality of induced oxidative DNA damage in nondividing neural cells. *Nucleic Acids Res.*, **36**, 5111–5121.
43. El Khamisy,S.F., Saifi,G.M., Weinfeld,M., Johansson,F., Helleday,T., Lupski,J.R. and Caldecott,K.W. (2005) Defective DNA single-strand break repair in spinocerebellar ataxia with axonal neuropathy-1. *Nature*, **434**, 108–113.
44. Ahel,I., Rass,U., El-Khamisy,S.F., Katyal,S., Clements,P.M., McKinnon,P.J., Caldecott,K.W. and West,S.C. (2006) The neurodegenerative disease protein aprataxin resolves abortive DNA ligation intermediates. *Nature*, **443**, 713–716.
45. Petermann,E., Keil,C. and Oei,S.L. (2006) Roles of DNA ligase III and XRCC1 in regulating the switch between short patch and long patch BER. *DNA Repair (Amst)*, **5**, 544–555.
46. Parsons,J.L., Dianova,I.I., Allinson,S.L. and Dianov,G.L. (2005) DNA Polymerase beta Promotes Recruitment of DNA Ligase IIIalpha-XRCC1 to Sites of Base Excision Repair. *Biochemistry*, **44**, 10613–10619.
47. Okano,S., Lan,L., Caldecott,K.W., Mori,T. and Yasui,A. (2003) Spatial and temporal cellular responses to single-strand breaks in human cells. *Mol. Cell Biol.*, **23**, 3974–3981.
48. El Khamisy,S.F., Masutani,M., Suzuki,H. and Caldecott,K.W. (2003) A requirement for PARP-1 for the assembly or stability of XRCC1 nuclear foci at sites of oxidative DNA damage. *Nucleic Acids Res.*, **31**, 5526–5533.
49. Lan,L., Nakajima,S., Oohata,Y., Takao,M., Okano,S., Masutani,M., Wilson,S.H. and Yasui,A. (2004) In situ analysis of repair processes for oxidative DNA damage in mammalian cells. *Proc. Natl Acad. Sci. USA*, **101**, 13738–13743.
50. Goode,E.L., Ulrich,C.M. and Potter,J.D. (2002) Polymorphisms in DNA repair genes and associations with cancer risk. *Cancer Epidemiol. Biomarkers Prev.*, **11**, 1513–1530.
51. Hung,R.J., Hall,J., Brennan,P. and Boffetta,P. (2005) Genetic polymorphisms in the base excision repair pathway and cancer risk: a HuGE review. *Am. J. Epidemiol.*, **162**, 925–942.
52. Takanami,T., Nakamura,J., Kubota,Y. and Horiuchi,S. (2005) The Arg280His polymorphism in X-ray repair cross-complementing gene 1 impairs DNA repair ability. *Mutat. Res.*, **582**, 135–145.
53. Qu,T., Morii,E., Oboki,K., Lu,Y. and Morimoto,K. (2005) Micronuclei in EM9 cells expressing polymorphic forms of human XRCC1. *Cancer Lett.*, **221**, 91–95.
54. Pachkowski,B.F., Winkel,S., Kubota,Y., Swenberg,J.A., Millikan,R.C. and Nakamura,J. (2006) XRCC1 genotype and breast cancer: functional studies and epidemiologic data show interactions between XRCC1 codon 280 His and smoking. *Cancer Res.*, **66**, 2860–2868.
55. Leng,S., Cheng,J., Pan,Z., Huang,C., Niu,Y., Dai,Y., Li,B., He,F. and Zheng,Y. (2004) Associations between XRCC1 and ERCC2 polymorphisms and DNA damage in peripheral blood lymphocyte among coke oven workers. *Biomarkers*, **9**, 395–406.
56. Weng,Z., Lu,Y., Weng,H. and Morimoto,K. (2008) Effects of the XRCC1 gene-environment interactions on DNA damage in healthy Japanese workers. *Environ. Mol. Mutagen.*, **49**, 708–719.